Mathematics and Computers in Simulation 34 (1992) 51–79
North-Holland

A consistent baroclinic quasigeostrophic ocean model in multiply connected ocean domains

Emin Özsoy [1], Carlos J. Lozano and Allan R. Robinson

Department of Earth and Planetary Sciences, Harvard University, Pierce Hall, 29 Oxford Street, Cambridge, MA 02138, United States

Abstract

Özsoy, E., C.J. Lozano and A.R. Robinson, A consistent baroclinic quasigeostrophic ocean model in multiply connected ocean domains, Mathematics and Computers in Simulation 34 (1992) 51–79.

The Harvard ocean baroclinic quasigeostrophic model is further extended to enable the treatment of multiply connected domains with arbitrary coastal boundary geometry. A set of sufficient quasigeostrophic boundary conditions at physical boundaries are determined by requiring consistency with a regular asymptotic expansion in the Rossby number of the primitive equations. To take advantage of fast Helmholtz solvers in regular domains, the physical multiply connected domain is embedded in a regular grid, and boundary conditions are imposed by using a variation of the capacitance matrix method. The accuracy of the method is exhibited by comparison with exact solutions.

1. Introduction

The Harvard baroclinic quasigeostrophic model is an eddy-resolving open ocean model [13] used extensively to study oceanic dynamical processes [19] and in forecast and hindcast studies [21]. The numerical calibration of this model [7,13,21] has shown that it provides the efficiency and accuracy required in these applications.

In a previous work Milliff [15] extended the Harvard open ocean model to simply connected oceans with coasts. Here we continue this extension to multiply connected oceans (i.e., with islands) and irregular physical boundaries. In the extension from simply to multiply connected domains, Dirichlet boundary conditions are expressed indirectly in terms of line integrals around the boundaries. This indirect prescription of the Dirichlet data is necessary in order to construct a quasigeostrophic solution that represents the leading term in an asymptotic expansion in the Rossby number to the primitive equations [11]. It is in this context that we call the set of conditions specifying the Dirichlet data at closed coastal boundaries (islands or a closed outer boundary) consistency conditions. In the numerical algorithms the core of our work is the following. The quasigeostrophic model requires at each time cycle the solution of a

[1] Present address: Institute of Marine Sciences, Middle East Technical University, P.K. 28, Erdemli, Içel 33731 Turkey.

set of elliptic problems. In a regular rectangular domain, advantage is taken of fast Helmholtz solvers, and in extending the model to irregular physical boundaries in a multiply connected ocean, we extended Milliff's modified capacitance method preserving the efficiency and accuracy of the direct method. The extension of direct solvers to accommodate irregular domains is well known [1], and here we develop a further variation of the capacitance matrix method [25], initiated by Milliff [14,15], which incorporates in the capacitance matrix the indirect prescription of the consistency conditions. In addition the time step algorithm (prognostic) of the Harvard model is modified in order to satisfy boundary conditions at irregular boundaries. This new development remedies undesirable vorticity transports across physical boundaries present in Milliff's model.

Capacitance methods have been previously employed for this problem. In early implementations [8,12] of full nonlinear baroclinic quasigeostrophic models the capacitance methods were based upon the work of Buzbee et al. [1] and applied to eddy-resolving basin-wide simulations on simply connected and single island domains. For later implementations of this approach, due essentially to Holland [8,9], see [4]. For another related implementation see [16]. The main differences in our approach from previous work are our ability to include islands within closed, semi-closed or open ocean outer boundaries. For all of these cases we determine a sufficient set of integral constraints for a well-posed problem and a simple and robust algorithm. Finally, in the numerical implementation, following [14], these constraints are incorporated into the capacitance matrix.

In Section 2 we introduce the initial boundary value problem for the baroclinic quasigeostrophic model as the leading approximation in the Rossby number to an initial boundary value problem for the primitive equations and derive a complete set of boundary conditions asymptotically consistent with this reference problem. Subgrid effects are modeled with a scale selective Shapiro filter [22]. The algorithm of the modified capacitance matrix method for multiply connected domains is presented in Section 3. In Section 4 we compare the model with an exact solution due to Flierl [5] of a linear baroclinic problem corresponding to quasigeostrophic free modes in an annulus. Our test runs serve to demonstrate the potential efficiency and accuracy of the model and, in addition, have enabled us to calibrate the model for enclosed, semi-closed and open oceans where islands play a dominant kinematic and dynamic role, e.g., the Eastern Mediterranean. Our final discussion and conclusions are given in Section 5. Details of derivation and numerical algorithms are relegated to the appendices.

2. Quasigeostrophic initial boundary value problem

In this section we state the problem to be solved and show that our selection of boundary conditions provides a sufficient set of boundary conditions to render the problem well posed. In this paper we consistently use nondimensional variables unless stated otherwise.

2.1. Ocean domain

The ocean domain is approximated by a cylinder with horizontal area D confined between the ocean surface $z = 0$, and a bottom surface $z = -1 + \epsilon\eta(x, y)$, with small topographic variations $\epsilon\eta(x, y)$ measured from a mean depth of $z = -1$. The horizontal domain geome-

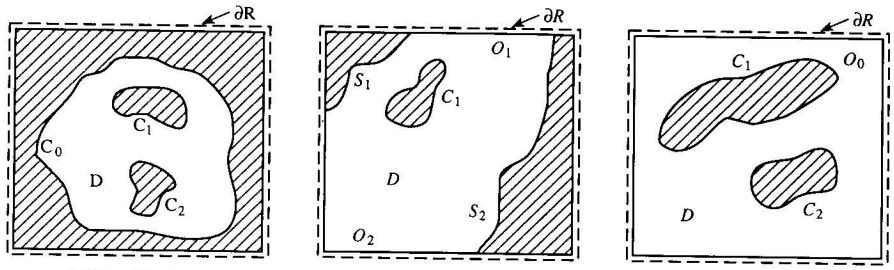

Fig. 1. Schematization of multiply connected domains: (a) enclosed, (b) semi-closed and (c) open outer boundaries.

tries are shown in Fig. 1. For modeling purposes we assume the fluid domain D to be embedded in a rectangular region R with boundary ∂R. In the case of the enclosed geometry in Fig. 1(a), closed coastal boundaries interior to ∂R are represented as C_j, $j = 0, \ldots, M$, C_0 being the outer basin boundary, and C_j, $j = 1, \ldots, M$, the M island boundaries interior to C_0. In the case of the semi-closed geometry in Fig. 1(b), the outer boundary consists of open segments O_k, $k = 1, \ldots, L$, and adjoining coastal segments S_k, $k = 1, \ldots, L$, where L is the number of segments. Finally, for open oceans in Fig. 1(c), the outer boundary O_0 coincides with ∂R.

2.2. The quasigeostrophic model

The quasigeostrophic equations are the leading terms of a uniform asymptotic expansion in the Rossby number ϵ of the primitive equations. In order to clarify the specification of the boundary conditions we outline a brief derivation. For details the reader is referred to [6,11,17,21]. Our starting point is the (nondimensional) equations of motion of incompressible water over a rotating Earth where the beta plane, hydrostatic and Boussinesq approximations have been introduced:

$$\epsilon(\boldsymbol{u}_t + \alpha \boldsymbol{u} \cdot \nabla \boldsymbol{u}) + (1 + \epsilon\beta y)\hat{k} \times \boldsymbol{u} = -\nabla p + \epsilon \boldsymbol{f}, \tag{2.1a}$$

$$p_z - \delta = 0, \tag{2.1b}$$

$$\nabla \cdot \boldsymbol{u} + \epsilon w_z = 0, \tag{2.1c}$$

$$\delta_t + \alpha \boldsymbol{u} \cdot \nabla \delta + \left[\left(\Gamma^2 \sigma(z) \right)^{-1} + \epsilon \alpha \delta_z \right] w = d, \tag{2.1d}$$

where $\boldsymbol{u}$ is the horizontal velocity, p the pressure and δ the buoyancy (proportional to negative density perturbation), ∇ denotes the horizontal gradient and subscripts denote differentiation. The local vertical component of the Earth's rotation varies as $\epsilon\beta y\hat{k}$ with meridional distance y, and $\hat{k}$ is a unit vector pointing upwards. The Rossby number ϵ is a small parameter measuring the relative importance of inertial as compared to rotational effects, and α is the ratio of the inertial to advective time scales. The background density stratification is represented by $\Gamma^2\sigma(z)$, where the constant Γ^2 scales its strength and $\sigma(z)$ is its local order 1 vertical variation. $\boldsymbol{f}$ and d are the body force and buoyancy source, respectively.

The vertical velocity w is already scaled by ϵ to reflect the fact that w is one order smaller than the horizontal velocity. Assuming a regular asymptotic expansion in ϵ for the variables $\boldsymbol{u}$, w, p and δ (e.g., $\boldsymbol{u} = \boldsymbol{u}^{(0)} + \epsilon \boldsymbol{u}^{(1)} + \mathrm{O}(\epsilon^2)$), we obtain from (2.1)

$$\frac{\partial Q}{\partial t} + \alpha \nabla \cdot \left(Q \boldsymbol{u}^{(0)} \right) = 0, \tag{2.2a}$$

where

$$Q = \zeta + \alpha^{-1} \beta y, \tag{2.2b}$$

$$\zeta = \nabla^2 \psi + \left(\Gamma^2 \sigma \psi_z \right)_z. \tag{2.2c}$$

The relative and thermal vorticity, the first and second terms respectively in (2.2c), depend upon the state of motion. The potential vorticity Q is formed from these contributions and the planetary vorticity, the second term in (2.2b). Here $\psi = p^{(0)}$ is the streamfunction related to the leading term in the horizontal velocity by

$$\boldsymbol{u}^{(0)} = \hat{k} \times \nabla \psi. \tag{2.2d}$$

For later reference, in terms of the density anomaly $\rho = \Gamma^2 \sigma \psi_z$, the vertical velocity is given by

$$w^{(0)} = -\left[\rho_t + \alpha \boldsymbol{u}^{(0)} \cdot \nabla \rho \right] + \Gamma^2 \sigma d, \tag{2.3a}$$

and its vertical derivative defines the first-order horizontal divergence

$$\nabla \cdot \boldsymbol{u}^{(1)} = -w_z^{(0)}. \tag{2.3b}$$

2.3. Boundary conditions

The boundary conditions at the top and bottom of the ocean are obtained using a classical asymptotic analysis of Ekman frictional layers [17]:

$$w^{(0)} = -\left(\frac{\partial}{\partial t} + \alpha \boldsymbol{u}^{(0)} \cdot \nabla \right) \rho_s = \hat{k} \cdot \nabla \times \boldsymbol{\tau}, \qquad \text{on } z = 0, \tag{2.4a}$$

$$w^{(0)} = -\left(\frac{\partial}{\partial t} + \alpha \boldsymbol{u}^{(0)} \cdot \nabla \right) \rho_b = E^{1/2}\, \hat{k} \cdot \nabla \times \boldsymbol{u}^{(0)} + \boldsymbol{u}^{(0)} \cdot \nabla \eta, \qquad \text{on } z = -1, \tag{2.4b}$$

where the Ekman number E is a nondimensional measure of the vertical diffusivity of momentum, $\rho_s = \Gamma^2 \sigma \, \partial \psi / \partial z \,|_{z=0}$, $\rho_b = \Gamma^2 \sigma \, \partial \psi / \partial z \,|_{z=-1}$.

At open boundaries, we require the Charney, Fjortoft and von Neumann [2,13] conditions, namely flow is prescribed everywhere in the boundary and vorticity is prescribed at inflow:

$$\psi = \psi_0(x, y, t), \quad \text{on } O_k, \ k = 1, \ldots, L, \tag{2.5a}$$

$$Q = Q_0(x, y, t), \quad \text{if } \boldsymbol{u}^{(0)} \cdot \hat{n} < 0 \text{ on } O_k, \ k = 1, \ldots, L, \tag{2.5b}$$

where $\hat{n}$ is the outward pointing normal vector to O_k. For semi-closed basins (Fig. 1(b)), the boundary condition on the coastal segments S_k are no inflow into the boundary and, following

[18], the streamfunction is continuous at the intersection of open boundaries with coastal boundaries:

$$\boldsymbol{u}^{(0)} \cdot \hat{n} = \nabla\psi \cdot \hat{s} = 0, \quad \psi = \psi_k^* \text{ on } S_k, \ k = 1, \ldots, L, \tag{2.5c}$$

where $\hat{s}$ is the tangential unit vector to S_k, ψ_k^* is the limit of the streamfunction along the adjacent open boundary O_k or O_{k-1} to S_k as it approaches the coastal segment S_k.

At all coastal closed boundaries (islands, coastal outer boundary) we require the kinematic condition of no flux normal to the coasts:

$$\boldsymbol{u}^{(0)} \cdot \hat{n} = \nabla\psi \cdot \hat{s} = 0, \quad \text{on } C_j, \ j = 1, \ldots, M. \tag{2.6}$$

Additional boundary conditions depend upon the physical parametrization of $\boldsymbol{f}$ and d in terms of the state variables. For instance, if one assumes $\boldsymbol{f} = K\nabla^2\boldsymbol{u}$, then a possible boundary condition is a no-slip condition [11]. In our derivation we find it convenient to keep the body force $\boldsymbol{f}$ and remove buoyancy sources d, whereas in our numerical implementation we do not include internal buoyancy sources, so $d^{(0)} = 0$, and dissipation, so $\boldsymbol{f}^{(0)} = 0$. In the time step algorithm for the potential vorticity, instead of dissipation, we employ a scale selective Shapiro filter [22], removing vorticity cascaded to grid resolution [10].

The problem of interest for a semi-closed ocean is the initial boundary value problem for the reduced set of equations (2.2), including the boundary conditions (2.4)–(2.6) with initial conditions

$$\psi = \psi_{\text{in}}, \quad \text{for } t = t_0, \tag{2.7a}$$

$$\rho_{\text{s}} = \rho_{\text{s,in}} \quad \text{at } z = 0, \quad \rho_{\text{b}} = \rho_{\text{b,in}} \text{ at } z = -1, \qquad \text{for } t = t_0. \tag{2.7b}$$

The enclosed basin initial boundary value problem can be obtained from the previous problem by removing (2.5) and extending (2.6) to include the outer boundary ($j = 0, \ldots, M$).

2.4. Additional boundary conditions: the consistency conditions

As it stands, the initial-value problem stated above does not have a unique solution since (2.6) can be satisfied by specifying the streamfunction ψ at closed coastal boundaries C_j as arbitrary functions of time and depth $\psi_{C_j}(t, z)$. It is of importance to notice at this point that once the functions ψ_{C_j} have been selected (with appropriate smoothness conditions), then the initial boundary value problem stated in Section 2.3 is well-posed, except for rather pathological cases. We now remove the indeterminacy in the selection of the functions $\psi_{C_j}(t, z)$ by requiring consistency with higher-order terms of the original primitive equation problem.

Assuming a uniform asymptotic expansion over the domain D (i.e., no boundary layers are formed in D), the first-order terms in the momentum equation (2.1a) are

$$\frac{\partial}{\partial t}\boldsymbol{u}^{(0)} + (\alpha\nabla^2\psi + \beta y)\hat{k} \times \boldsymbol{u}^{(0)} + \hat{k} \times \boldsymbol{u}^{(1)} = -\nabla\left(p^{(1)} + \tfrac{1}{2}\alpha\boldsymbol{u}^{(0)} \cdot \boldsymbol{u}^{(0)}\right) + \boldsymbol{f}^{(0)}.$$

Letting again $\hat{s}$, $\hat{n}$ be the unit tangent and normal vectors to a closed path C contained in D, the line integral of the above equation along C yields

$$\oint_C \boldsymbol{u}^{(1)} \cdot \hat{n} \, \mathrm{d}l = \frac{\partial}{\partial t}\oint_C \boldsymbol{u}^{(0)} \cdot \hat{s} \, \mathrm{d}l - \oint_C \boldsymbol{f}^{(0)} \cdot \hat{s} \, \mathrm{d}l - \oint_C (\alpha\nabla^2\psi + \beta y)\boldsymbol{u}^{(0)} \cdot \hat{n} \, \mathrm{d}l, \tag{2.8a}$$

where we have used $\hat{k} \times \boldsymbol{u} \cdot \hat{s} = -\boldsymbol{u} \cdot \hat{n}$ and assumed that the first-order pressure function $p^{(1)}$ is single valued; furthermore, if the contour C coincides with an island C_j, $j = 1, \ldots, M$, or a closed outer boundary C_0, then the local kinematic conditions

$$\boldsymbol{u}^{(0)} \cdot \hat{n} = \boldsymbol{u}^{(1)} \cdot \hat{n} = 0 \tag{2.8b}$$

simplify (2.8a) to:

$$\frac{\mathrm{d}\gamma_j(t)}{\mathrm{d}t} = \oint_{C_j} f^{(0)} \cdot \hat{s} \, \mathrm{d}l, \tag{2.9a}$$

where

$$\gamma_j(t) = \oint_{C_j} \nabla\psi \cdot \hat{n} \, \mathrm{d}l \tag{2.9b}$$

is the quasigeostrophic circulation at time t over the coastal boundary C_j.

At the initial time t_0 the quasigeostrophic circulation

$$\gamma_j(t_0) = \oint_{C_j} \nabla\psi_{in} \cdot \hat{n} \, \mathrm{d}l \tag{2.9c}$$

is known; thus the circulation at time t depends, in a unique fashion, upon the initial circulation and the line integral of $f^{(0)}$ around C_j over previous times.

We show in the next subsection that for semi-closed basins the quasigeostrophic circulations $\gamma_j(t)$ determine uniquely the streamfunction values at coastal boundaries $\psi_{C_j}(t, z)$. For enclosed basins, other than an additive constant, a similar result holds. This constant has no bearing on the dynamics [1].

2.4.1. Modal representation

At this point, it is convenient to introduce the modal representation of the solution in preparation for the proof of the statement above and to the numerical algorithms.

The eigenfunctions of the Sturm–Liouville boundary problem

$$\frac{\mathrm{d}}{\mathrm{d}z}\left(\sigma \frac{\mathrm{d}S^{[m]}}{\mathrm{d}z}\right) = -\left(\frac{\lambda}{\Gamma}\right)^2 S^{[m]}, \quad -1 < z < 0, \qquad \frac{\mathrm{d}S^{[m]}}{\mathrm{d}z}(-1) = \frac{\mathrm{d}S^{[m]}}{\mathrm{d}z}(0) = 0$$

form a complete set of functions and the corresponding eigenvalues $\lambda_{[0]} = 0 < \lambda_{[1]} < \cdots < \lambda_{[l]} < \cdots$ are simple [17]. The first mode $\lambda_{[0]} = 0$ is called barotropic; the remaining baroclinic. In the modal representation ψ and ζ are given by [2]

$$\psi = \sum_{m \geq 0} \psi^{[m]}(x, y, t) S^{[m]}(z), \tag{2.10a}$$

$$\zeta = \sum_{m \geq 0} \zeta^{[m]}(x, y, t) S^{[m]}(z). \tag{2.10b}$$

[1] However, if the rigid lid approximation implied in (2.4a) is relaxed, then the choice of the constant is no longer arbitrary.

[2] This is strictly correct for the case of constant top and bottom density. For variable top and bottom density, modifications are required including additional terms in the elliptic problems; but these additional terms do not alter the solvability arguments or the numerical solution procedures.

In the modal representation equations (2.2c), (2.5a), (2.5c), (2.6) and (2.9) lead us to the family of elliptic problems

$$\nabla^2 \psi^{[m]} - \left(\lambda_{[m]}\right)^2 \psi^{[m]} = \zeta^{[m]}, \tag{2.11}$$

with boundary conditions

$$\psi^{[m]} = \psi_0^{[m]}, \quad \text{on } O_k, \ k = 1, \ldots, L, \tag{2.12a}$$

at open boundaries,

$$\nabla \psi^{[m]} \cdot \hat{s} = 0, \quad \psi^{[m]} = \psi^{*[m]} \text{ on } S_k, \ k = 1, \ldots, L, \tag{2.12b}$$

on coastal segments of semi-closed domains; and for enclosed basins the barotropic component ($m = 0$) at the outer boundary satisfies

$$\psi^{[0]} = 0, \quad \text{on } C_0, \tag{2.12c}$$

whereas the baroclinic components ($m > 0$) satisfy

$$\nabla \psi^{[m]} \cdot \hat{s} = 0, \quad \text{on } C_0, \tag{2.12d}$$

$$\gamma_0^{[m]}(t) = \gamma_0^{[m]}(t_0) + \int_{t_0}^{t} \oint_{C_0} f^{[m]} \cdot \hat{s} \, \mathrm{d}l \, \mathrm{d}t. \tag{2.12e}$$

Finally for all islands ($j > 0$),

$$\nabla \psi^{[m]} \cdot \hat{s} = 0, \quad \text{on } C_j, \tag{2.13a}$$

$$\gamma_j^{[m]}(t) = \gamma_j^{[m]}(t_0) + \int_{t_0}^{t} \oint_{C_j} f^{[m]} \cdot \hat{s} \, \mathrm{d}l \, \mathrm{d}t. \tag{2.13b}$$

Here $\gamma_j^{[m]}$ is the quasigeostrophic circulation around the boundary C_j of the modal streamfunction $\psi^{[m]}$.

In Appendix A we show that these boundary value problems have unique solutions.

3. The modified capacitance matrix method: multiple coast segments and multiply connected domains

In the Harvard open ocean quasigeostrophic model the potential vorticity Q is advanced in time using the discrete version of (2.2a) (prognostic) and then the new streamfunction is computed in the modal representation (diagnostic). The detailed description of the numerical algorithms for the Harvard quasigeostrophic open ocean model can be found in [7,13]. Here we give a brief description of the algorithm.

Grid

The model uses in the horizontal a rectangular grid R_h with a constant grid spacing h. In the vertical the grid is nonuniform and set up at K levels $z_k = -H_k$, $k = 0, \ldots, K-1$.

Let ψ_k denote the values of ψ at $z = z_k$, $k = 0, \ldots, K-1$, and let

$$\zeta_k = \zeta(z_k), \quad k = 1, \ldots, K-2,$$

$$\zeta_0 = \zeta(z_0) + \frac{\rho_s}{H_0}, \qquad \zeta_{K-1} = \zeta(z_{K-1}) - \frac{\rho_b}{H_{K-1} - H_{k-2}}.$$

In the initial boundary value problem, we seek to determine $(\zeta_0, \ldots, \zeta_{K-1})$, ρ_s, ρ_b satisfying the evolution equations (2.2a), with $Q_k = \zeta_k + \alpha^{-1}\beta y$, (2.4), initial conditions (2.7) and the boundary conditions (2.5), (2.6), and consistency conditions (2.11), (2.12).

Prognostic

The discretization of (2.2a) and (2.4) uses a fourth-order accurate finite element in space, and a second-order accurate Adams–Bashforth time difference scheme. The updated values $(\zeta_0, \ldots, \zeta_{K-1})$, ρ_s, ρ_b at each time step are passed through Shapiro filters [22] to remove high wavenumbers ($\sim$ 2–4 grid points).

Diagnostic

The new prognostic values $(\zeta_0, \ldots, \zeta_{K-1})$, ρ_s, ρ_b are transformed to the truncated (K terms) modal representation (2.10) and the resulting elliptic problems (2.11)–(2.13) are solved via the algorithm in Section 3.3. The model uses a fast Helmholtz solver based on block cyclic reduction [23] amenable to vector and parallel implementation [24]. The solver is used twice; in the second pass the method of deferred corrections is used in order to attain fourth-order accuracy consistent with the space discretization used in (2.2a) and (2.4).

Our extension to the open ocean model includes modifications to the time stepping algorithm in order to account for physical boundaries in the interior of the domain; thus, the computational molecules at physical boundaries satisfy boundary conditions and potential vorticity is filtered in the physical domain only (including physical boundaries). This modification was not included in Milliff's implementation [15].

We now proceed to present the numerical solution of the baroclinic and barotropic elliptic boundary value problems (2.11)–(2.13). For the sake of simplicity, throughout this section we drop the index $[m]$ distinguishing the modes, and we separate the cases for enclosed and semi-closed or open oceans only when it becomes pertinent.

3.1. Discrete domain and boundaries

We denote by R_h a grid in a rectangular domain R (Fig. 2) with grid spacing h. From here on the subscript h denotes functions defined on that grid. The discrete projection of the fluid domain D on this grid system is a subset D_h of R_h. A boundary segment of D is approximated by grid points along a staircase curve formed by picking the closest successive pairs of nodes along the grid lines. In the semi-closed case the outer boundary is made up of open boundary segments $O_{h,k}$ contained in the boundary set ∂R_h of R_h, and solid segments $S_{h,k}$, $k = 1, \ldots, L$. The interior boundaries are islands $C_{h,j}$, $j = 1, \ldots, M$. The sets $S_{h,k}$ and $C_{h,j}$ must be contained in the interior $R_h^I = R_h - \partial R_h$ of R_h. For enclosed basins there are $M+1$ coastal segments $C_{h,j}$, $j = 0, \ldots, M$. We denote by $C_h^T = \cup_j C_{h,j}$ the union of all closed coastal segments and let $M = |C_h^T|$ denote the total number of grid points at closed coastal boundaries. The union of all

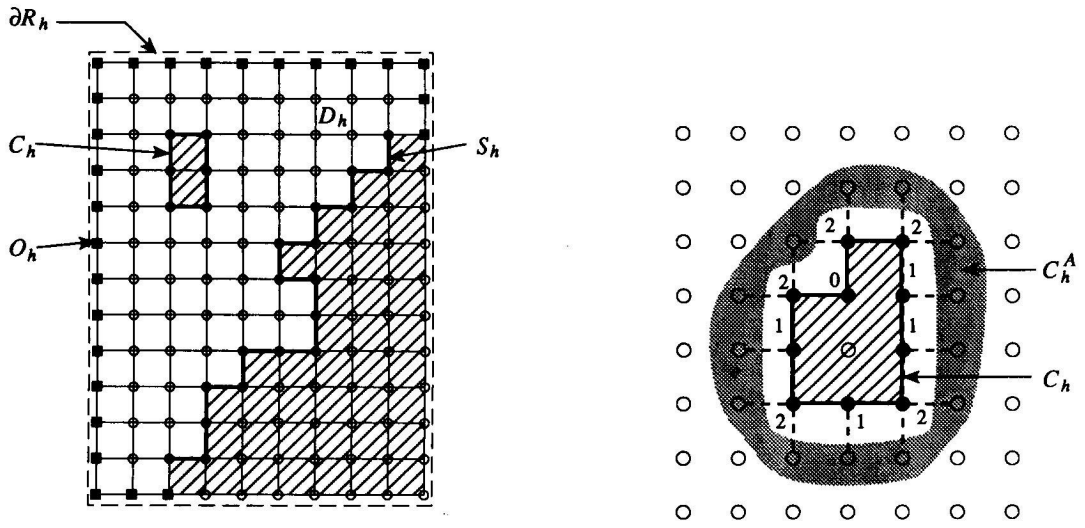

Fig. 2. Schematization of the discrete rectangular grid R_h and the boundaries (a), and the adjacent set C_h^A to the closed boundary segment C_h (b). The number next to a boundary point is its number of neighbors in the interior of D_h.

coastal boundaries is denoted by $\mathscr{C}_h^T = (\cup_{k=1,\ldots,L} S_{h,k}) \cup (\cup_{k=1,\ldots,M} C_{h,k})$ and $\mathscr{M} = |\mathscr{C}_h^T|$ the total number of boundary grid points.

3.2. Discrete boundary value problem

In the physical interior D_h we approximate (2.11) using the standard five-point Laplacian K_h:

$$K_h[\psi_h(i)] - \lambda^2 \psi_h(i) = \zeta_h(i), \quad i \in D_h. \tag{3.1}$$

For semi-closed basins the boundary conditions (2.12a), (2.12b) are cast in the form

$$\psi_h(i) = (\psi_0)_h(i), \quad i \in O_{h,k}, \tag{3.2a}$$

at open outer boundaries. At solid outer boundary segments, with $i_{1,\ldots,i_l}$ denoting successive grid points in $S_{h,k}$, the boundary condition (2.5c) is

$$\psi_h(i_p) = \psi_h(i_{p+1}), \quad p = 1,\ldots,l-1, \tag{3.2b}$$

$$\psi_h(1) = (\psi_0)_h(\hat{1}), \tag{3.2c}$$

where $\hat{1}$ is the grid point adjacent to $i_1 \in S_{h,k}$ and belonging to an open boundary segment; $(\psi_0)_h(\hat{1})$ is the prescribed boundary condition at this open segment grid point and $k = 1,\ldots,L$. The barotropic enclosed boundary condition (2.12c) is written similarly to (3.2b), (3.2c), and the conditions (2.13a) are written similarly to (3.2b).

The discrete analog of the quasigeostrophic circulation integral (2.9b) of a closed boundary $C_{h,j}$ is formed as follows. Each grid point $i \in C_{h,j}$ has either 0, 1 or 2 neighboring points, along

the axes, lying in the interior of the physical domain D_h (see Fig. 2(b)). Letting

$$\gamma_{h,j,i} = \sum_{i_l} [\psi_h(i) - \psi_h(i_l)], \tag{3.3a}$$

where the summation over i_l extends over the interior neighboring points if any. The discrete quasigeostrophic circulation integral along $C_{h,j}$ is now given by

$$\gamma_{h,j} = \sum_{i \in C_j} \gamma_{h,j,i}. \tag{3.3b}$$

Finally, we specify the consistency (inviscid) condition (2.13b)

$$\gamma_{h,j} = \gamma_j, \quad j = 1, \ldots, M. \tag{3.3c}$$

The definition (3.3a), (3.3b) of the circulation integral is motivated as follows. Complementing the definition (3.3a), (3.3b), with similar definitions of the discrete circulation integrals $\gamma^{O}_{h,k}, \gamma^{S}_{h,k}$ along open and semi-closed boundaries respectively, it is simple to show that the discrete Green theorem

$$\sum_{i \in D_h^I} K_h[\psi_h(i)] h^2 = \sum_{k=0}^{L} (\gamma^{O}_{h,k} + \gamma^{S}_{h,k}) + \sum_{j=1}^{M} \gamma_{h,j}, \tag{3.4a}$$

for semi-closed domains, and

$$\sum_{i \in D_h^I} K_h[\psi_h(i)] h^2 = \sum_{j=0}^{M} \gamma_{h,j}, \tag{3.4b}$$

for enclosed domains, holds. Here D_h^I are the physical grid points not at the boundary of D_h. In addition, a discrete analog of the first Green identity (A.5) holds; and, as a result, the solvability of the discrete elliptic boundary value problems can be proved as in Appendix A.

3.3. Modified capacitance matrix algorithm

Let again R_h^I and ∂R_h denote the set of interior grid points and boundary points of R_h, respectively. We associate to the discrete boundary value problem (3.1)–(3.3) the following functions in R_h.

The discrete Green functions Φ_h

For each grid point l on the solid boundaries $\mathscr{C}_h^T$ we define a discrete Green function on R_h given by

$$\begin{aligned} &K_h[\Phi_h(i, l)] - \lambda^2 \Phi_h(i, l) = \delta_h(i, l), && \text{for } i \in R^I, \\ &\Phi_h(i, l) = 0, && \text{for } i \in \partial R_h. \end{aligned} \tag{3.5}$$

Here the Kronecker delta $\delta_h(i, l)$ takes the value zero for $i \in R_h$ everywhere, except at the grid point $i = l$ where it takes the value 1.

A particular solution

Let ζ_h^I denote a function defined over R_h^I such that it coincides with the right-hand side ζ_h of (3.1) in D_h; and let ψ_h^B be defined over ∂R_h such that it coincides with the right-hand side of (3.2) over $O_{h,k}$. A particular solution ψ_h^P is the discrete function satisfying

$$\begin{aligned} &K[\psi_h^P(i)] - \lambda^2 \psi_h^P(i) = \zeta_h^I(i), \quad i \in R^I, \\ &\psi_h^P(i) = \psi_h^B(i), \qquad\qquad i \in \partial R_h. \end{aligned} \tag{3.6}$$

The ansatz

We now propose a solution to (3.1), (3.2) and (3.4) of the form

$$\psi_h(i) = \psi_h^P(i) + \sum_{l \in C_h^T} w_h(l) \Phi_h(i, l), \quad i \in R_h. \tag{3.7}$$

In view of (3.5) and (3.6) the proposed function (3.7) satisfies (3.1) and (3.2a) for arbitrary extensions of ζ_h to the nonphysical domain, and for arbitrary values of the function w_h defined on $\mathscr{C}_h^T$. In passing we notice that the second term $\hat{\Phi} = \sum_{l \in \mathscr{C}_h^T} w_h(l) \Phi_h(i, l)$ is the solution to

$$K_h[\hat{\Phi}_h(i)] - \lambda^2 \hat{\Phi}_h(i) = \sum_{l \in C_h^T} w_h(l) \delta_h(i, l), \quad \text{for } i \in R^I, \tag{3.8a}$$

$$\hat{\Phi}_h(i, l) = 0, \qquad \text{for } i \in \partial R_h, \tag{3.8b}$$

thus representing the response to vorticity point sources of strength w_h distributed over $\mathscr{C}_h^T$.

Algorithm

In order to satisfy the remaining boundary conditions we substitute (3.7) into (3.2b) and (3.4) obtaining precisely $\mathscr{M} = |\mathscr{C}_h^T|$ equations for $\mathscr{M}$ vorticity point sources w_h:

$$\boldsymbol{G}_h w_h = r_h. \tag{3.9}$$

For details in the assembling of matrix $\boldsymbol{G}$ see Appendix B. The matrix $\boldsymbol{G}_h$ is nonsingular and its coefficients are independent of the inhomogeneous terms in (3.2b) and (3.3c); thence it can be inverted for each geometry once and for all.

In our implementation the matrix $\boldsymbol{G}_h^{-1}$, the modified capacitance matrix, is computed once per mode $[m]$ and model geometry and then stored.

At each time step cycle and for each mode $[m]$ our method proceeds as follows:

(a) the particular solution ψ_h^P is obtained solving (3.6) with the fast Helmholtz solver with two passes;

(b) the right-hand side r_h of (3.9) is assembled and the vorticity point sources $w_h = \boldsymbol{G}_h^{-1} r_h$ are computed; and

(c) ψ_h is found by using the Helmholtz solver for the problem

$$K_h[\psi_h(i)] - \lambda^2 \psi_h(i) = \zeta_h^I(i) + \sum_{l \in C_h^T} w_h(l) \delta_h(i, l), \quad i \in R^I, \tag{3.10a}$$

$$\psi_h = \psi_h^B \in \partial R_h. \tag{3.10b}$$

Algorithm overhead

The computational overhead of the method is as follows. The computation of the capacitance matrix G_h^{-1} requires $\mathscr{M}$ applications of the fast Helmholtz solver to determine the discrete Green functions $\Phi_h[l]$ for each grid point $l \in C_h^T$ at closed coastal boundaries and the inversion of G_h. During computational cycles the storage of the capacitance matrix is required. At each computational time cycle the fast Helmholtz solver is required to solve (3.6) and (3.10); thus the number of passes through the solver are $\frac{3}{2}$ as many as for the open ocean model. The computational cost assembling the residual r_h and computing the vorticity point sources w_h is nominal.

4. Numerical experiments

In this section we discuss a set of numerical experiments aimed to test the model implementation by reproducing an analytical solution of Flierl [5] in a multiply connected domain, and we illustrate the application of the model to a realistic ocean model simulation.

4.1. Linear, baroclinic free modes in an annulus

A two-level ocean ($K = 2$) occupies an annular domain $\hat{r} < r < 1$, with $r = (x^2 + y^2)^{1/2}$, $0 < \hat{r} < 1$, without any surface or bottom forcing ($\rho_s = \rho_b = 0$). For this problem, the regime is linear ($\alpha = 0$) and there is no interior dissipation ($f^{(0)} = 0$). To set the numerical model we select levels $z_1 = -\frac{1}{4}$, $z_2 = -\frac{3}{4}$ and $\sigma = 1$ to find the eigenvalues $\lambda_{[0]} = 0$, $\lambda_{[1]} = \Gamma$. The solution to (2.2a) of interest is the pure baroclinic mode $\psi^{[1]} = \frac{1}{2}(\psi_1 - \psi_2)$ such that $\psi_1 = -\psi_2$ and $\psi^{[0]} = \frac{1}{2}(\psi_1 + \psi_2) \equiv 0$. The time-periodic streamfunction is

$$\psi^{[1]} = \Re\{F(x, y)e^{-i(\mu x + \omega t)}\}, \tag{4.1}$$

with F satisfying

$$\nabla^2 F - \nu^2 F = 0, \quad \nu^2 = \Gamma^2 - \mu^2, \quad \mu = \frac{2\beta}{\omega}. \tag{4.2}$$

The boundary conditions (2.11) in terms of F are

$$F = c_1 e^{-i\mu r \cos\theta}, \quad \text{at } r = 1, \qquad F = c_{\hat{r}} e^{-i\mu r \cos\theta}, \quad \text{at } r = \hat{r}, \tag{4.3a,b}$$

where c_1 and $c_{\hat{r}}$ are undetermined coastal constants. The boundary conditions (2.13) read

$$\int_0^{2\pi} e^{-i\mu r \cos\theta} \frac{\partial F}{\partial r} d\theta = 0, \quad \text{at } r = \hat{r} \text{ and } r = 1. \tag{4.4a,b}$$

The relationships (4.3) and (4.4) are satisfied for a countable number of eigenfrequencies, and for each eigenfrequency ω, there is a unique ratio of amplitudes $c_1/c_{\hat{r}}$. The amplitude at one of the coasts is fixed by the initial conditions. In our simulations we use the largest eigenfrequency ω_1, except for one case where we use the second eigenfrequency ω_2. The solution for F is expressed in terms of Bessel and trigonometric series [5].

4.2. Numerical solution of the Flierl's problem

From (4.1) we see that the solution is a Rossby wave traveling east with wavenumber μ and frequency ω modulated by an amplitude function $F(x, y)$. Figure 3 shows the computed and analytical streamfunction and vorticity at time $\frac{3}{4}T$ and T for an ocean with an opening at the western boundary along the line $x = -\frac{26}{30}$. The analytical solution satisfies (4.1)–(4.4), whereas the numerical solution satisfies (4.1)–(4.3) and (4.4b). At the outer open boundary (4.4a) is replaced by the continuity condition (2.5c); at the open boundary we use the open boundary condition (2.5) with ψ_0 and Q_0 given by the analytical solution. In the following semi-closed basins (S) experiments, the analytical and numerical solutions are obtained in a similar fashion.

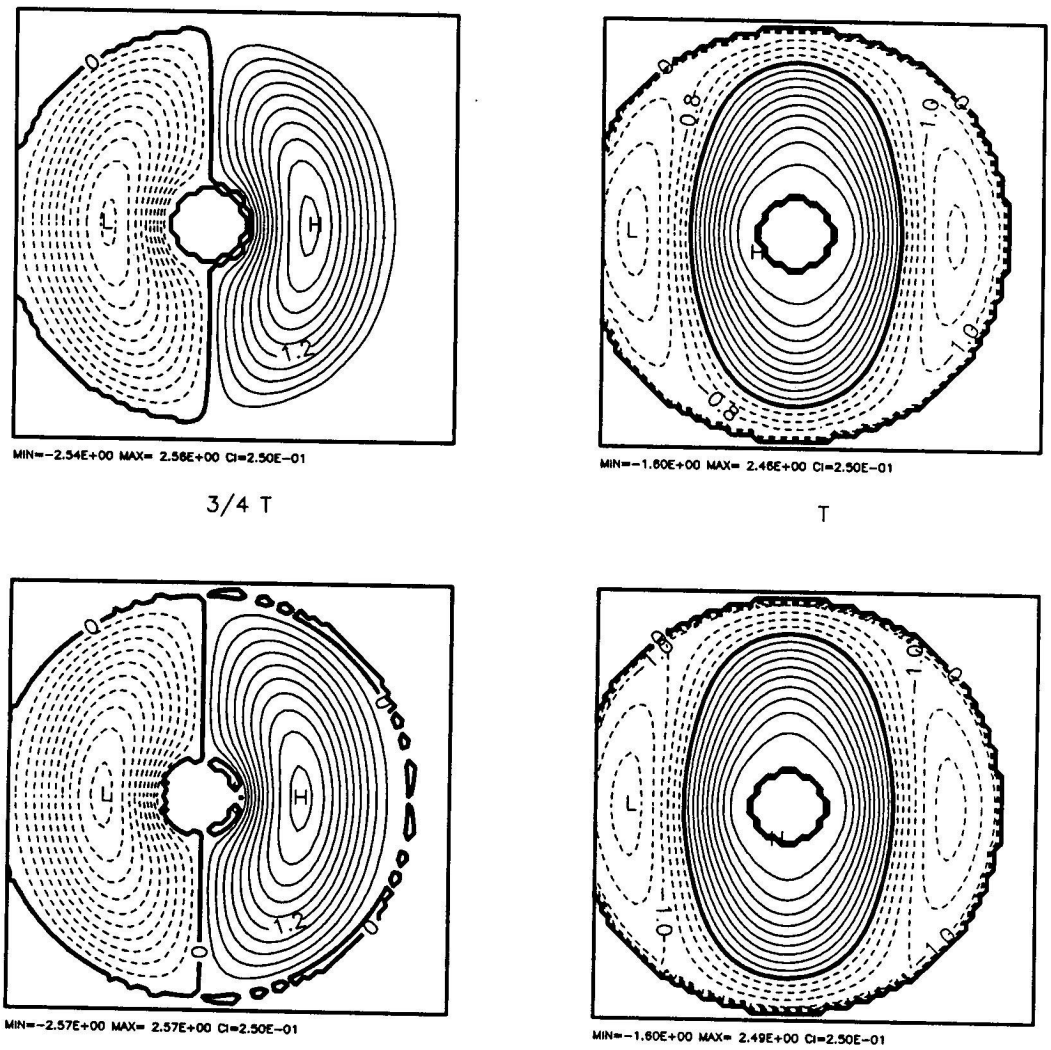

Fig. 3(a). Numerical (top panels) and analytical (bottom panels) streamfunction at times $\frac{3}{4}T$ (left panels) and T (right panels) where T is the period, and for $\Gamma^2 = 10$, $\hat{r} = 0.2$.

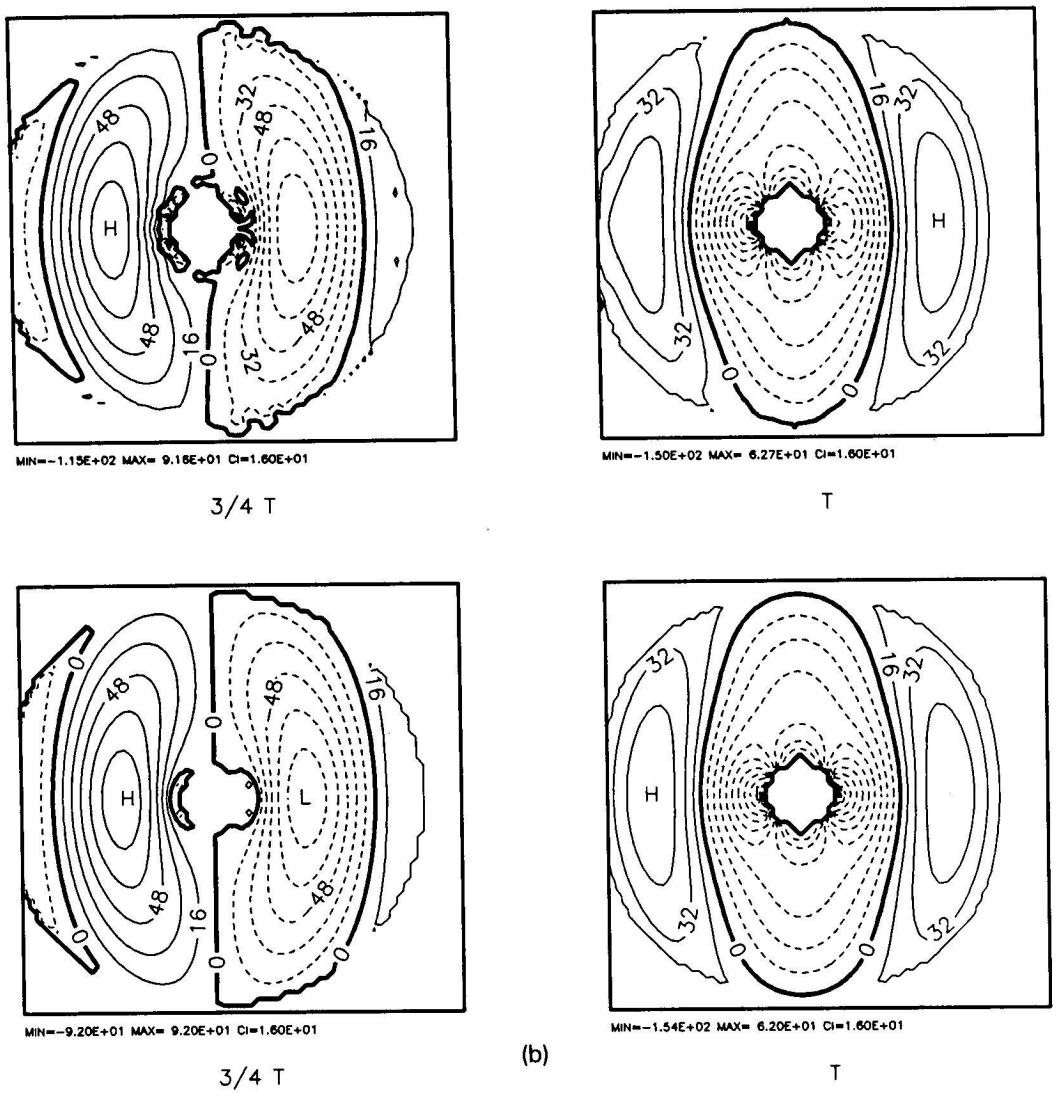

(b)

Fig. 3(b). Same as in Fig. 3(a) for vorticity.

A selection of the numerical experiments carried out is summarized in Table 1. We selected $\beta = 1$, and using the basin radius $r = 1$ as a horizontal length scale, the grid size $\Delta x = \frac{1}{30}$. Space and time resolutions are characterized, for consistency with [21], using $\tau = \frac{1}{4}T\ \Delta t = \frac{1}{2}\pi\omega\ \Delta t$ and $\nu = 2\pi/(\mu \cdot 4\ \Delta x) = \frac{1}{4}\omega\pi\ \Delta x$, where τ is the number of time intervals in a quarter period and ν is the number of space intervals per quarter wavelength, respectively. The selection of τ and ν was based upon the findings in [15] and a set of test runs with free Rossby waves (not shown) using similar physics ($\alpha = 0$, $\beta = 1$). Our experiments were determined to be satisfactory when the root mean square errors RMSE for the streamfunction and vorticity were similar to the equivalent free Rossby waves experiments. The analytical series solutions have a good convergence with about 20 terms in the series in all cases except for $\Gamma^2 = 80$. For this case we accepted errors in the analytical solution of about 5 percent. In all these runs the Shapiro filter

Table 1
Model runs summary of comparison with analytic solutions

Run	Domain type [a]	Stratification Γ^2	Island radius $\hat{r}$	Time step τ	Grid size ν	Maximum ψ	RMSE [b] ζ
A	E	10	0.0	20	3.0	0.03 [1] 0.13 [5]	0.06 [1] 0.14 [5]
B	S	10	0.2	10	2.9	0.04 [1] 0.05 [5]	0.09 [1] 0.10 [5]
C	E	10	0.2	10	2.9	0.02 [1] 0.036 [5]	0.08 [1] 0.09 [5]
D	E	10	0.2	5	2.9	0.16 [1] 0.22 [5]	0.27 [1] 0.4 [5]
E [c]	E	10	0.2	5	2.4	0.14 [1] 0.63 [5]	0.17 [1] 0.64 [5]
F [c]	E	10	0.2	20	2.4	0.12 [1] 0.54 [1]	0.13 [1] 0.52 [5]
G	S	80	0.2	25	1.2	0.15 [1] 0.27 [2]	0.17 [1] 0.30 [2]
H	E	80	0.2	10	1.2	0.09 [1] 0.20 [2]	0.11 [1] 0.21 [2]
I	E	50	0.2	37.5	1.5	0.11 [1] 0.20 [2]	0.12 [1] 0.22 [2]
J	E	50	0.2	25	1.5	0.13 [1] 0.20 [2]	0.20 [1] 0.22 [2]
K	E	10	0.6	30	1.9	0.11 [1] 0.15 [1]	0.12 [1] 0.22 [2]
L	E	10	0.6	20	1.9	0.11 [1] 0.15 [1]	0.12 [1] 0.22 [2]

[a] E = enclosed, S = semi-closed domain.
[b] The number in brackets is the number of periods of integration for which the maximum error is reported.
[c] For second eigenfrequency.

was disabled. The physical parameters Γ^2 and the island size $\hat{r}$ were selected to reproduce similar results in Flierl's examples and Milliff's experiments [14], and extended to other regimes of oceanographic interest. In Table 1 we report the maximum normalized root mean square error (RMSE) in streamfunction and vorticity observed in a given number of periods. The error tendencies are better observed in the RMSE time histories shown for instance in Fig. 4.

Run A is for a simply connected basin $\hat{r} = 0$ with $\Gamma^2 = 10$ and reproduces a numerical experiment in [14]. The growth of the error trend shown in [14, Fig. 13C] persists if the solution is continued for several periods using the previous algorithm. Replacing the algorithm with our new implementation we are able to reduce the errors and maintain the low level of error for the entire length of the experiment (5 periods). We attribute the improvement to a correction

in the evaluation of the circulation integral of [14] (see Appendix B), and to the control of vorticity leakage across boundaries achieved by the modification of the time step algorithm.

A comparison between semi-closed and enclosed configurations indicates that no significant error differences occur. This is illustrated for the worst case, runs G and H in Figs. 5 and 6. Previous experiments (not shown) with a correct circulation integral but with no vorticity leakage correction show systematically larger errors and noticeable discrepancies between the enclosed and semi-closed configuration.

Starting with experiment C, a series of runs varying frequency (E and F), Γ^2 (I and J) and island radius (K and L) show reasonable errors despite coarser spatial resolution τ. Figures 7 and 8 show the fields and associated RMSE errors for two different geometries and two stratifications, runs C, I and L.

The error dependence in the parameter τ is illustrated in Fig. 9 for $\Gamma^2 = 10$, $\hat{r} = 0.2$. Detailed analyses of the fields both for these experiments and the free Rossby waves show that the discrete phase speed is slightly faster than the analytical phase speed leading to phase shifting and is, in part, responsible for error growth.

4.3. Real ocean data application

The first application of the new model to real ocean data initialization and simulation is in the Levantine Basin of the Eastern Mediterranean Sea. This is an interesting test of the model because the coastlines, an island (Cyprus) and topography present complex constraints to a flow field which is composed itself of a rich set of interconnected subbasin scale gyres and jets [20]. We demonstrate here a simulation initialized with the objectively analyzed observations from the multiple ship cooperative survey of the POEM (Physical Oceanography of the Eastern Mediterranean) program on November 1985. Figure 10 shows the main thermocline ($z = -80m$) streamfunction after 5 days. The resolution is 5 km ($\nu \sim 5$–30) and the time step 2 hours is limited by the Courant–Friedrichs–Lewy condition. The dynamically adjusted features maintain the overall structure of the observations, and are remarkably stable and robust in 45 day runs. Robust and semi-permanent anticyclones are observed in the Southern portion with motions penetrating below the thermocline. The Northern flows are separated by meandering currents and filaments eventually approaching the Cyprus region where different recirculation regimes are established. To the North of the Eastward meandering current cyclonic and anticyclonic eddies accompanied by strong coastal currents interact. The permanent cyclone in the Northeast portion of the basin, the Rhodes gyre, as well as the Anaximander eddy are well represented in this run.

5. Discussion and conclusions

The extensions to the Harvard quasigeostrophic model numerical algorithms to accommodate arbitrary coastal boundaries, namely the modified capacitance matrix algorithm for multiply connected domains and time stepping algorithm in an irregular domain, are efficient (Section 3.3) and comparisons with exact linear solutions (Section 4) show good convergence in regimes of oceanographic interest.

Fig. 4.

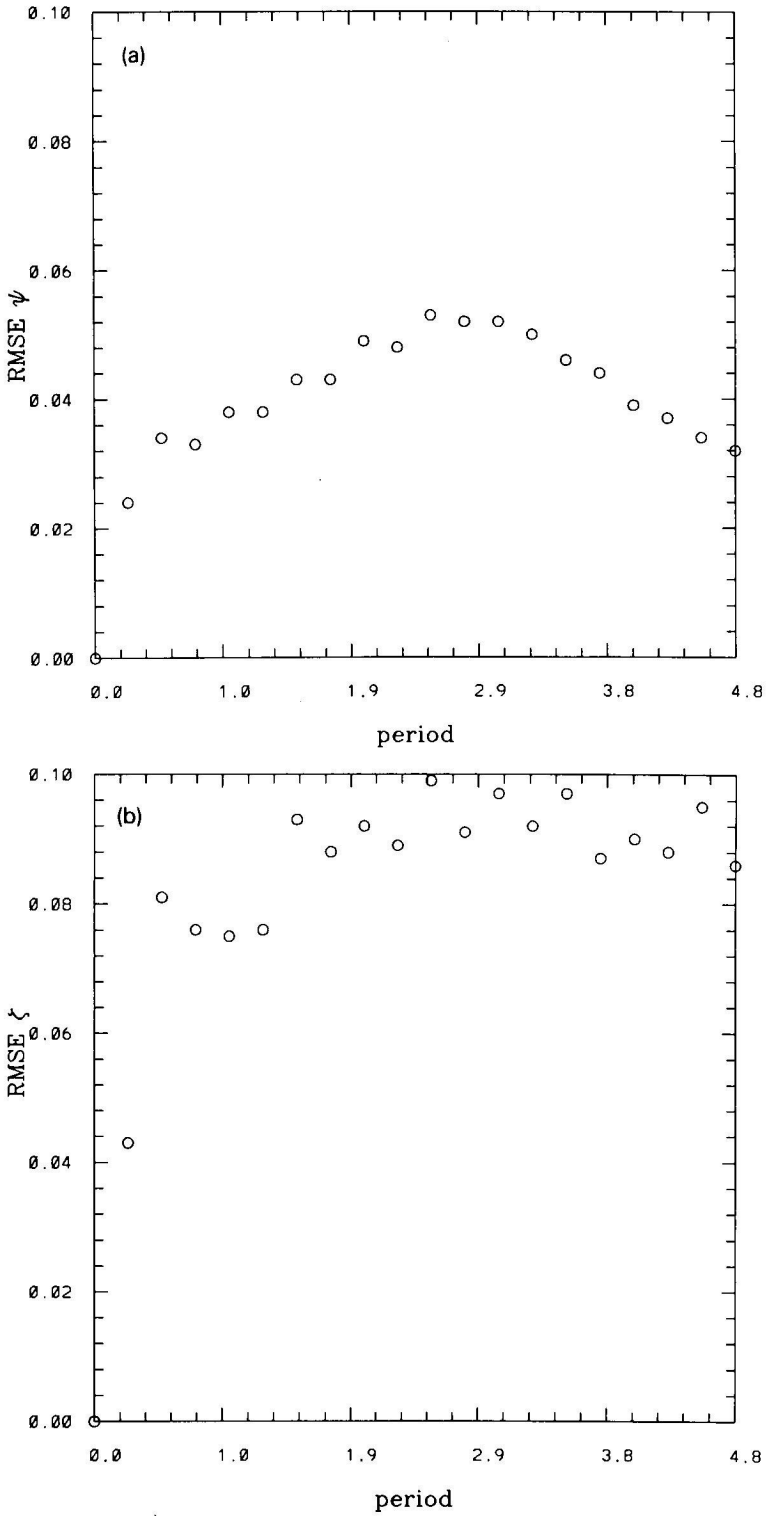

Fig. 4. Normalized root mean square errors RMSE in streamfunction (a) and vorticity (b) for five periods with $\Gamma^2 = 10$, $\hat{r} = 0.2$, $\tau = 10$, $\nu = 2.9$.

Solvability for the elliptic problems in the quasigeostrophic initial boundary value problem consistent with a primitive equations (PE) initial boundary problem has been established. Previous authors ([11,18] and others) have proposed various sets of consistent boundary conditions without proof of solvability. It follows from our proof that the various sets of conditions proposed by McWilliams [11] are solvable; albeit complicated. In the process of establishing solvability (Appendix A) we have constructed influence functions (A.1) that are utilized in Holland's capacitance matrix algorithm [8]. Here the use of the circulation matrix (A.4) provides some simplifications to their approach.

The computation of quasigeostrophic circulation integrals at coastal boundaries along coasts with tortuous geometry must be avoided. In this case it is desirable to compute the circulation integral, using the divergence theorem, in terms of an interior circulation and area integral.

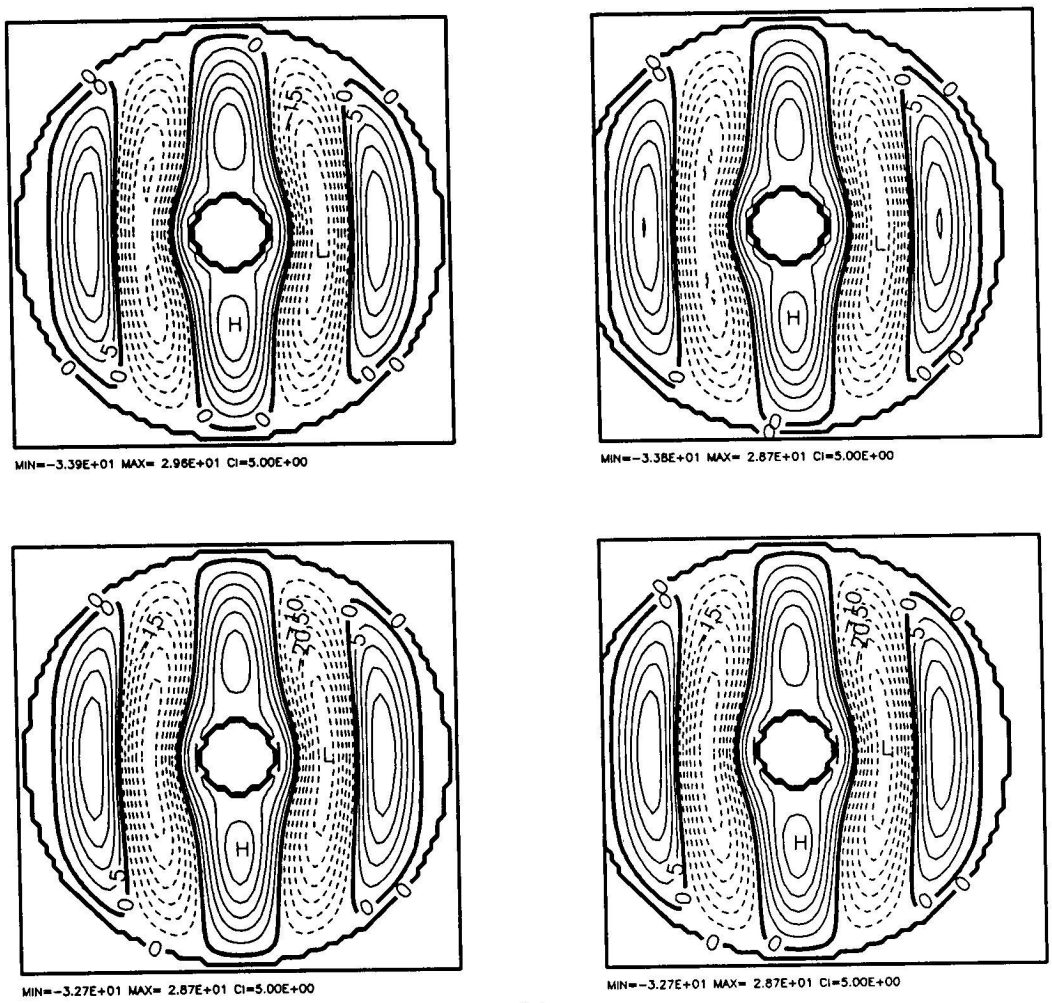

(a)

Fig. 5(a). Numerical (top panels) and analytical (bottom panels) for enclosed (left panels) and semi-closed (right panels) streamfunctions with $\Gamma^2 = 80$, $\hat{r} = 0.2$.

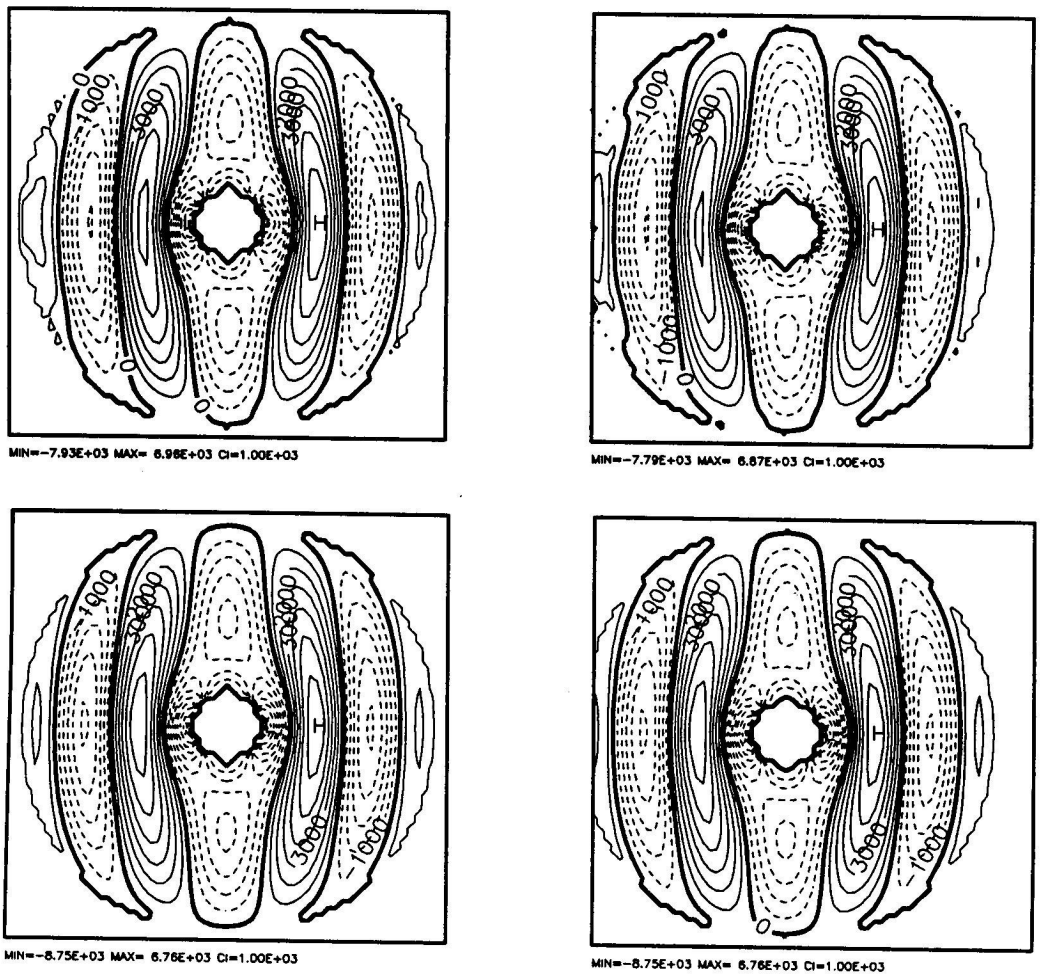

(b)

Fig. 5(b). Same as in Fig. 5(a) for vorticity.

The modified capacitance matrix formulation is no longer feasible under these circumstances and alternative formulations like the circulation matrix formulation become necessary.

Another approach is to map the physical domain to a more regular domain. For simply connected domains a capacitance method is no longer required, but for multiply connected domains the advantages of regular computational domains and a capacitance method can be combined with advantage.

In our determination of consistency conditions the essential additional information from higher-order terms was a kinematic condition (2.8b), namely no first-order fluxes across coastal boundaries. This fact gives us clues as to the limitations of the uniform asymptotic assumption, implicitly made in all previous derivations of consistency conditions for this problem. A parametrization of the dissipation of the form $f^{[0]} = \kappa \nabla^2 \boldsymbol{u}$ leads to the possible formation of lateral boundary layers breaking the uniform asymptotic assumption; thus consistency conditions in formulation using such parametrizations require revision.

In our approach the ocean is inviscid in the large energy containing scales and in the numerical model we have used a high wavenumber vorticity sweeper, the Shapiro filter, that does not develop boundary layers; nonetheless limitations remain. The idealization of coasts as vertical solid cylinders has additional obvious limitations. Certainly in this and similar models the intent is not to resolve coastal circulations, but to include the dominant effects of the lateral boundaries in the interior of the ocean. Further study is required to assess the effects of lateral boundary layer circulations in the presence of realistic coastal geometries to the interior ocean circulation.

Appendix A. Solvability of boundary value problem (2.11)–(2.13)

For convenience we drop the modal index $[m]$ in this section. Let ψ_p denote a particular solution [3] of (2.11), (2.12a)–(2.12d) and (2.13a) with $\psi_p = 0$ on C_i, where i runs over all closed coastal boundaries for baroclinic modes and all island boundaries for barotropic modes. We introduce the *influence functions* ϕ_i defined as the solution to

$$\nabla^2 \phi_i = \lambda^2 \phi_i, \tag{A.1}$$

taking the value 0 at all boundaries of D except at C_i where it takes the value 1. We propose a solution to (2.11)–(2.13) of the form

$$\psi = \psi_p + \sum_i \alpha_i \phi_i. \tag{A.2}$$

The function (A.2) satisfies (2.11) and (2.12a)–(2.12d) for arbitrary coefficients α_i and it will satisfy (2.12e) and (2.13b) provided

$$\gamma_j(t) = \oint_{C_j} \nabla \psi_p \cdot \hat{n}\, dl + \sum_i \alpha_i \oint_{C_j} \nabla \phi_i \cdot \hat{n}\, dl,$$

where j has the same range as the index i. For convenience, we rearrange this system of linear equations for α_i in the form

$$\sum_i \hat{\gamma}_{j,i}\, \alpha_i = \gamma_j(t) - \oint_{C_j} \nabla \psi_p \cdot \hat{n}\, dl, \tag{A.3}$$

where

$$\hat{\gamma}_{j,i} = \oint_{C_j} \nabla \phi_i \cdot \hat{n}\, dl \tag{A.4}$$

are the elements of the circulation matrix representing the circulation induced by ϕ_i on the boundary C_j. The linear system of equations (A.3) has a unique solution provided the circulation matrix is nonsingular. Below we prove a little bit more; namely, this matrix is

[3] This is not the same particular solution as defined in (3.6).

positive definite. To this end let us substitute the auxiliary function $\phi = \Sigma_i \beta_i \phi_i$ in the Green first identity

$$\int_D \left[(\nabla\phi)^2 + \phi\nabla^2\phi \right] \mathrm{d}a = \int_{\partial D} \phi \, \nabla\phi \cdot \hat{n} \, \mathrm{d}l, \tag{A.5}$$

where ∂D is the boundary of D, to obtain the relation

$$\sum_{i,j} \hat{\gamma}_{j,i} \beta_i \beta_j = \int_D \left[(\nabla\phi)^2 + (\lambda\phi)^2 \right] \mathrm{d}a, \tag{A.6}$$

where j, as above, has the same range as the index i.

For points in the unit sphere $\Sigma_i \beta_i^2 = 1$ the right-hand side of (A.6) is bounded away from zero if either (a) $\lambda \neq 0$ or (b) $\lambda = 0$ and $\cup_i C_i \neq \partial D$. That is, the circulation matrix $\hat{\gamma}_{j,i}$ for these two cases is positive definite. Before giving the proof, notice that (a) and (b) are satisfied in the baroclinic and barotropic boundary problems (2.11)–(2.13), respectively.

If (a), ϕ is not identically null in D, since it is continuous in D and up to the boundary, $\phi = \beta_i$ in C_i and there is an i with $\beta_i \neq 0$. It follows now that the second term in the right-hand side of (A.6) is bounded away from zero. If (b), the function ϕ is not a constant in D, since it is different from zero at some closed boundary and zero at a boundary which is not closed. Since ϕ is not a constant, there is a neighborhood in D for which $\nabla\phi$ is not null; and the first term in (A.6) is bounded away from zero.

The exceptional handling of the barotropic boundary value problem for enclosed basins stems from the fact that for this case the solution to the homogeneous problem with ϕ equal to a constant has zero circulation; thus if the circulation matrix is extended to include the outer closed boundary, then it is singular. Our approach reduces the barotropic enclosed basin problem to an equivalent *barotropic open basin.*

We can concisely summarize this appendix as follows. Baroclinic quasigeostrophic circulations map one-to-one to the corresponding baroclinic streamfunction values at closed coastal boundaries, and island barotropic quasigeostrophic circulations map one-to-one to barotropic streamfunction values at island boundaries.

Appendix B. Construction of the extended capacitance matrix

The matrix G_h is conveniently partitioned in blocks, each block associated with a coastal boundary segment. For each discrete closed boundary $C_{h,k}$ we associate to it the set of all interior points $C^{\mathrm{A}}_{h,k}$ of D_h adjacent to $C_{h,k}$ as in Section 3.3. Its union, denoted again by $C^{\mathrm{A}}_h = \cup_{k=1,\ldots,M} C^{\mathrm{A}}_{h,k}$ has $M_{\mathrm{A}} = |C^{\mathrm{A}}_h|$ grids points. The union of all coastal boundaries is denoted by $\mathscr{C}^{\mathrm{T}}_h = (\cup_{k=1,\ldots,L} S_{h,k}) \cup (\cup_{k=1,\ldots,M} C_{h,k})$.

With $B_{i,l} = \Phi_h(i, l)$, $W_l = w_h(l)$, we can write (3.7) in the form

$$\psi_h(i) = \psi^{\mathrm{P}}_h(i) + \sum_{l \in \mathscr{C}^{\mathrm{T}}_h} B_{i,l} W_l. \tag{B.1}$$

For each outer coast segment $S_{h,k}$ and each closed coastal segment $C_{h,k}$ substituting (B.1) in (3.2b) yields after some arrangement

$$\sum_{l \in \mathscr{C}^{\mathrm{T}}_h} (B_{i_m,l} - B_{i_{m+1},l}) W_l = r_{k,i_m}, \tag{B.2}$$

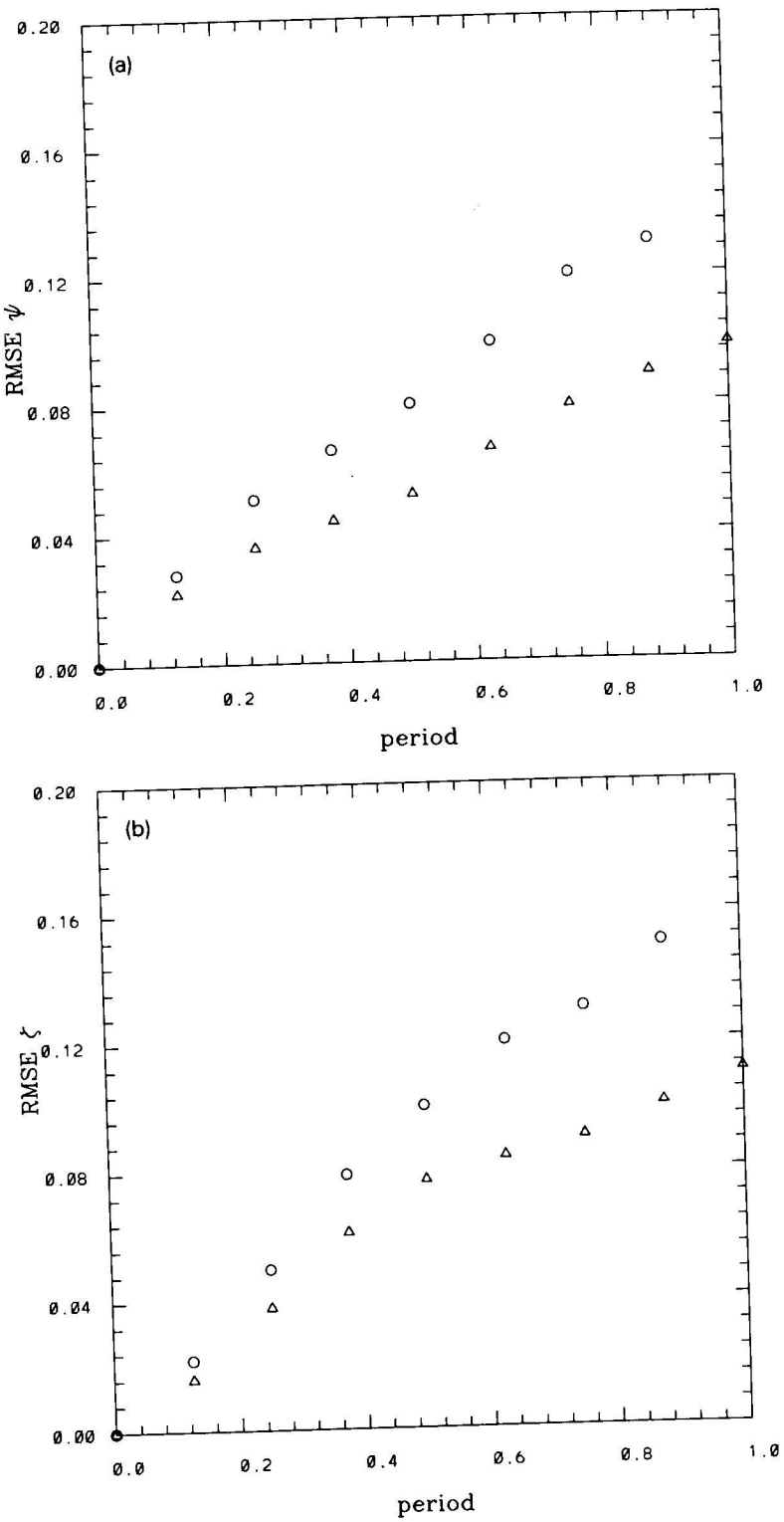

Fig. 6. Same as in Fig. 4 for one period, $\Gamma^2 = 80$, $\hat{r} = 0.2$; ($\triangle$) $\tau = 10$, enclosed, ($\circ$) $\tau = 25$, semi-closed.

Fig. 7(a

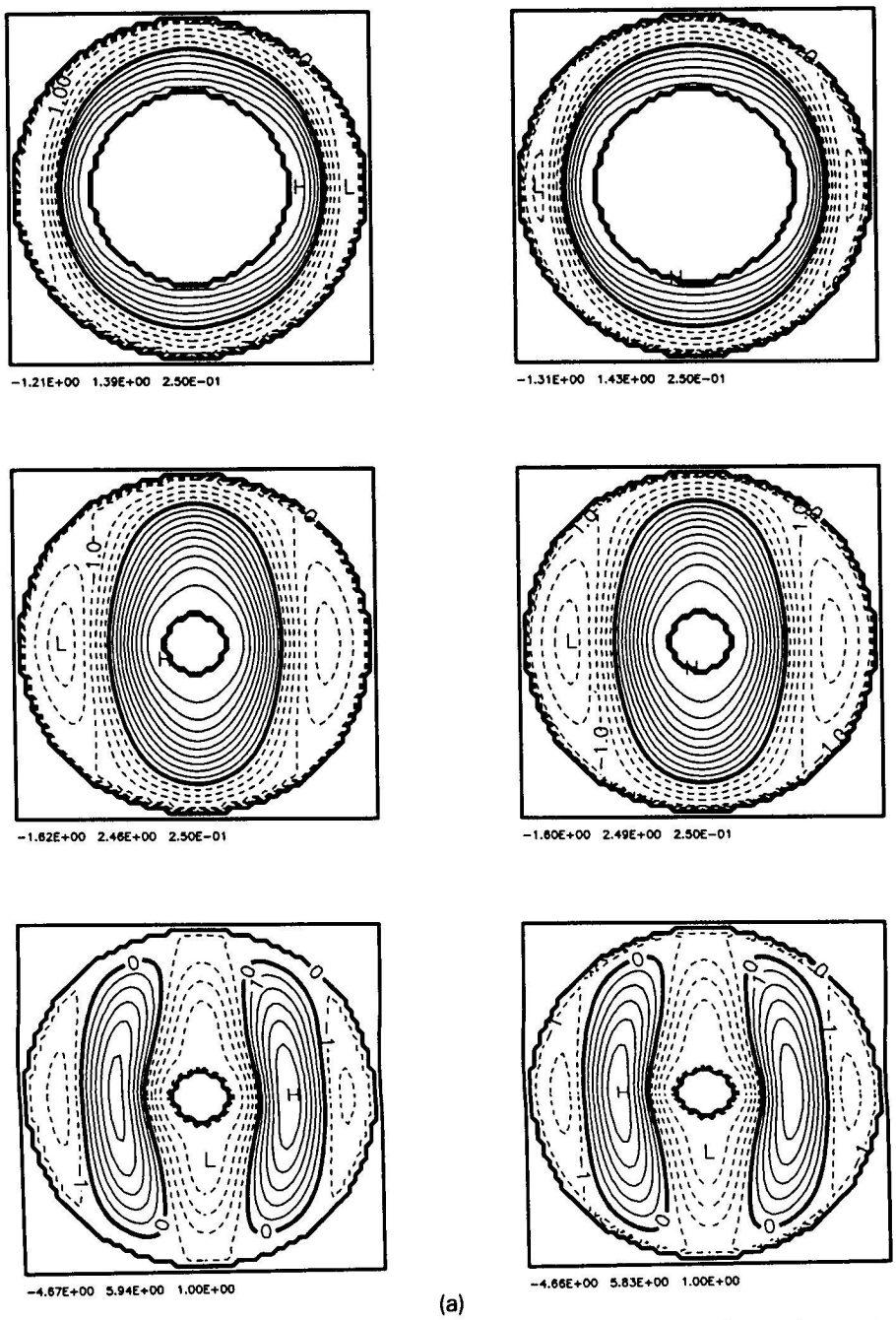

(a)

Fig. 7(a). Numerical (left panels) and analytical (right panels) streamfunction for $\Gamma^2 = 10$, $\hat{r} = 0.6$ (top), $\Gamma^2 = 10$, $\hat{r} = 0.2$ (middle), $\Gamma^2 = 50$, $\hat{r} = 0.2$ (bottom).

semi-closed.

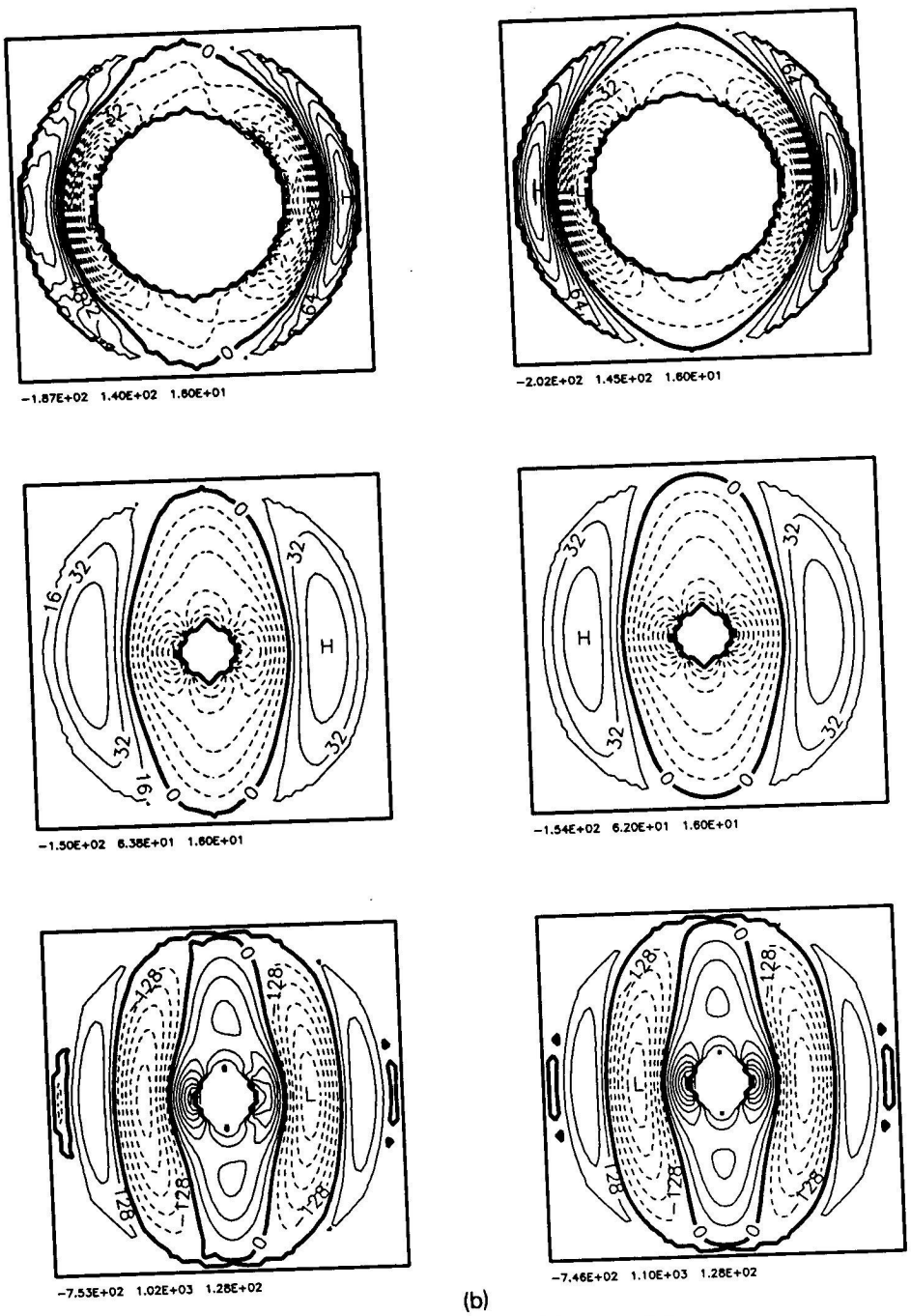

(b)

Fig. 7(b). Same as in Fig. 7(a) for vorticity.

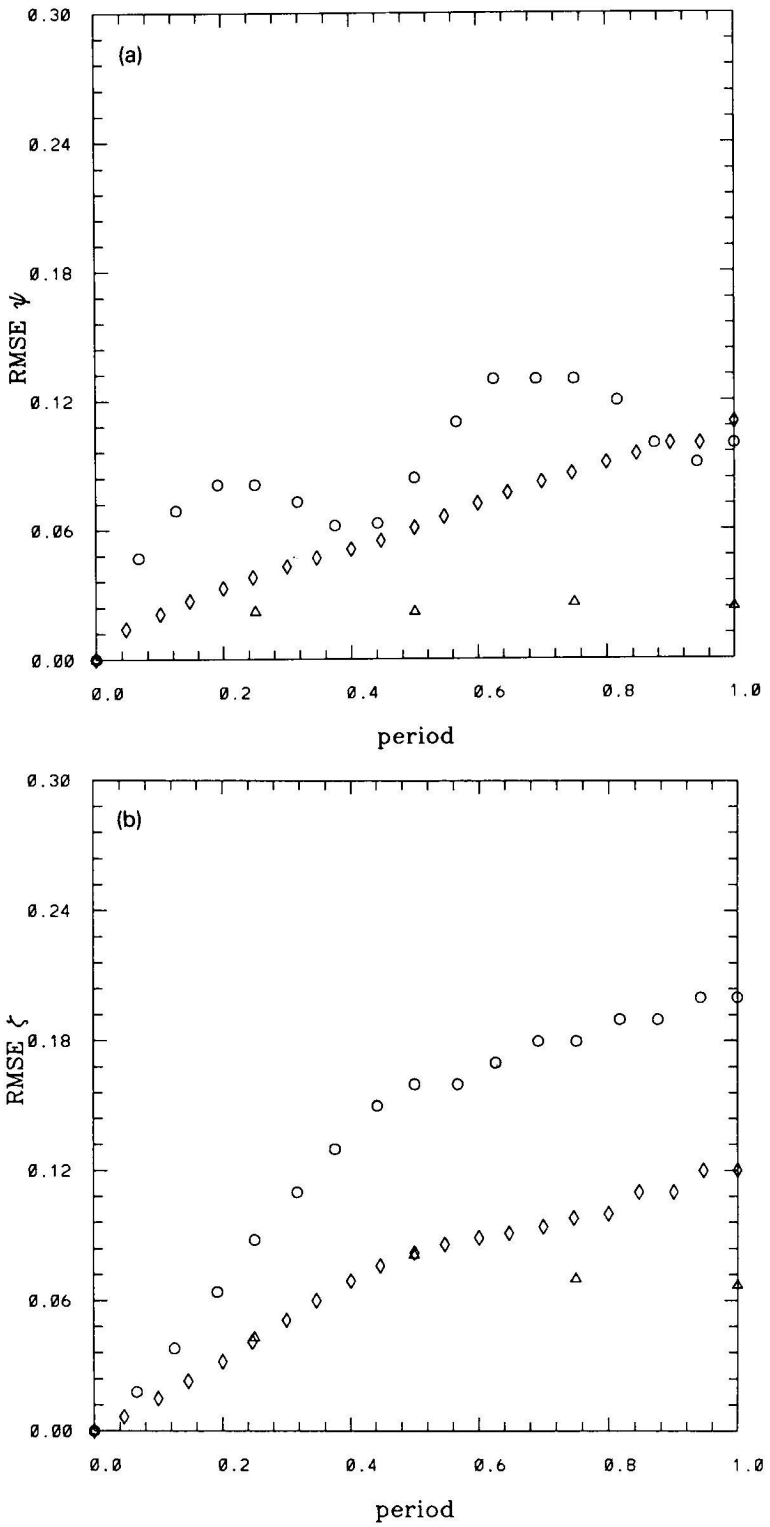

Fig. 8. Same as in Fig. 4 with ($\triangle$) $\Gamma^2 = 10$, $\hat{r} = 0.2$, ($\diamond$) $\Gamma^2 = 10$, $\hat{r} = 0.6$, ($\circ$) $\Gamma^2 = 50$, $\hat{r} = 0.2$.

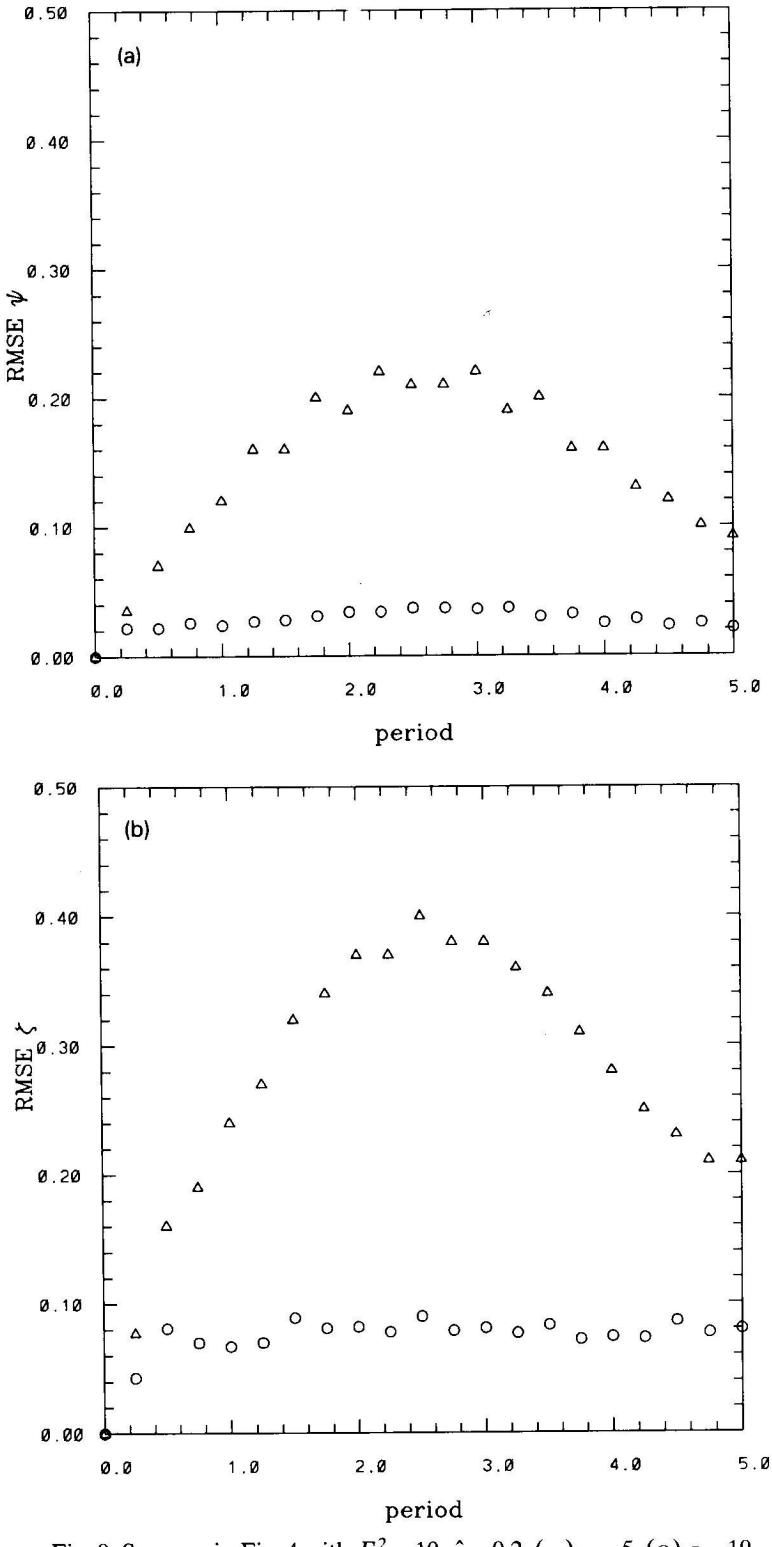

Fig. 9. Same as in Fig. 4 with $\Gamma^2 = 10$, $\hat{r} = 0.2$, ($\triangle$) $\tau = 5$, ($\circ$) $\tau = 10$.

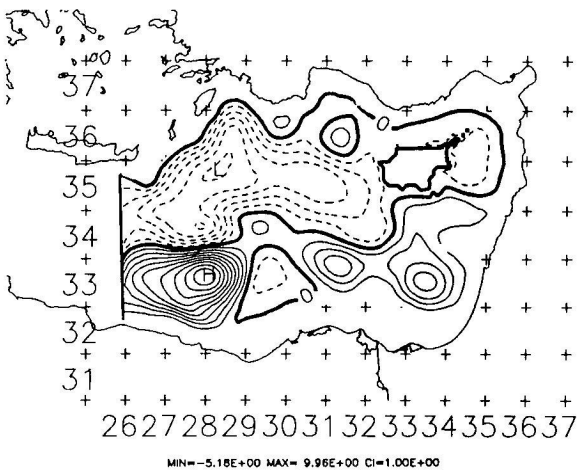

Fig. 10. Nondimensional streamfunction for the Eastern Levantine Mediterranean basin.

where the residual is given by

$$r_{k,i_m} = -\left(\psi_h^{\mathrm{P}}(i_m) - \psi_h^{\mathrm{P}}(i_{m+1})\right). \tag{B.3}$$

For each boundary segment $S_{h,k}$ there are precisely $|S_{h,k}|-1$ or $|C_{h,k}|-1$ relations (B.2).

For each outer coast segment the first point in the segment takes the value of its closest open boundary segment (3.2c), i.e.,

$$\sum_{l\in\mathscr{C}_h^{\mathrm{T}}} B_{i_1,l} W_l = r_{i_1,k}, \tag{B.4}$$

where

$$r_{k,i_1} = -\psi_h^{\mathrm{P}}(i_1) + (\psi_0)_h(\hat{1}). \tag{B.5}$$

For each island $C_{h,k}$ substitution of (B.1) in (3.3b) yields after some arrangement

$$\sum_{l\in\mathscr{C}_h^{\mathrm{T}}} \left(\sum_{i\in C_{h,k}} B_{i,l} - \sum_{i\in C_{h,k}^{\mathrm{A}}} B_{i,l} \right) W_l = r_{k,i_1}, \tag{B.6}$$

where the residual is given by

$$r_{k,i_1} = -\sum_{l\in\mathscr{C}_h^{\mathrm{T}}} \left(\sum_{i\in C_{h,k}} \psi_h^{\mathrm{P}} i - \sum_{i\in C_{h,k}^{\mathrm{A}}} \psi_h^{\mathrm{P}} i \right). \tag{B.7}$$

Equations (B.2), (B.4) and (B.6) form (3.9). In the code implementation each block can be assembled as in [14] after the terms in the left-hand side of (B.6) arising from contributions from interior grid points $C_{h,k}^{\mathrm{A}}$, omitted in [14], are included.

Acknowledgements

The initial stages of this work were carried out during a one-year visit to Harvard University by E. Özsoy, first as a Unesco grantee and later as a Fullbright scholar. The first author expresses his thanks to the Harvard University for support, and to Prof. Allan R. Robinson and his Harvard group for providing to him the ambiance of academic freedom and nourishment. Drs. Nadia Pinardi and Ralph Milliff provided enlightening discussions, Prof. Donald Anderson's review of an early draft helped to improve our presentation, Ms. Maryam Golnaraghi kindly provided the setup of the model in the Eastern Mediterranean and Mr. Wayne Leslie assisted in figure preparation. The research of A.R. Robinson and C.J. Lozano was supported by ONR grants N00014-90-J-1593 and University Research Initiative N00014-86-K-0751. The numerical work reported in this study was performed under grant HVD200 at the NSF Supercomputer Center San Diego CRAY Y-MP.

References

[1] B.L. Buzbee, G.H. Golub and C.W. Nielson, On direct methods for solving Poisson's equations, *SIAM J. Numer. Anal.* 7 (1970) 627–656.
[2] J.G. Charney, R. Fjortoft and J. von Neumann, Numerical integration of the barotropic vorticity equation, *Tellus 2* (1950) 237–254.
[3] J.G. Charney and G.R. Flierl, Oceanic analogues of large scale atmospheric motions, in: B.A. Warren and C. Wunsch, eds., *Evolution of Physical Oceanography* (MIT Press, Cambridge, MA, 1981) 504–550.
[4] P.F. Cummins and L.A. Mysak, A quasi-geostrophic circulation model of the Northeast Pacific. Part I: a preliminary numerical experiment, *J. Phys. Oceanogr.* 18 (1988) 1261–1286.
[5] G.R. Flierl, Simple applications of McWilliams's 'A note on a consistent quasigeostrophic model in a multiply connected domain', *Dynamics Atmospheres Oceans* 1 (1977) 443–453.
[6] H.P. Greenspan, *The Theory of Rotating Fluids* (Cambridge Univ. Press, London, 1969).
[7] D.B. Haidvogel, A.R. Robinson and E.E. Schulman, The accuracy, efficiency, and stability of three numerical models with application to open ocean problems, *J. Comput. Phys.* 34 (1980) 1–53.
[8] W.R. Holland, The role of mesoscale eddies in the general circulation of the ocean — numerical experiments using a wind-driven quasi-geostrophic model, *J. Phys. Oceanogr.* 8 (1978) 363–392.
[9] W.R. Holland, Quasi-geostrophic modeling of eddy-resolving ocean circulation, in: J.J. O'Brien, ed., *Advanced Physical Oceanographic Numerical Modeling* (Reidel, Dordrecht, 1986) 203–231.
[10] M.G. Marietta and A.R. Robinson, eds., Status and outlook of ocean modeling research dispersion and related applications, Sandia Report 85-2806, Sandia Laboratories, Albuquerque, NM, 1986.
[11] J.C. McWilliams, A note on a consistent quasigeostrophic model in a multiply connected domain, *Dynamics Atmospheres Oceans* 1 (1977) 427–441.
[12] J.C. McWilliams, W.R. Holland and J.H.S. Chow, A description of numerical circumpolar currents, *Dynamics Atmospheres Oceans* 2 (1978) 213–291.
[13] R.N. Miller, A.R. Robinson and D.B. Haidvogel, A baroclinic quasigeostrophic open ocean model, *J. Comput. Phys.* 50 (1981) 38–70.
[14] R.F. Milliff, Quasigeostrophic ocean flows in coastal domains, Ph.D. Thesis, Harvard Univ., Harvard Open Ocean Model Reports No. 34 (1989).
[15] R.F. Milliff, A modified Capacitance Matrix Method to implement coastal boundaries in the Harvard Open Ocean Model, *Math. Comput. Simulation* 31 (6) (1989/90) 541–564.
[16] A. Pares-Sierra and G.K. Valleis, A fast semi-direct method for the numerical solution of non-separable elliptic equations in irregular domains, *J. Comput. Phys.* 82 (2) (1989) 398–412.
[17] J. Pedlosky, *Geophysical Fluid Dynamics* (Springer, New York, 1983).

[18] N. Pinardi and R.F. Milliff, A note on consistent quasigeostrophic boundary conditions in partially open, simply and multiply connected domains, *Dynamics Atmospheres Oceans* 14 (1989) 65–76.
[19] N. Pinardi and A.R. Robinson, Quasigeostrophic energetics of open ocean regions, *Dynamics Atmospheres Oceans* 10 (1986) 185–221.
[20] A.R. Robinson, M. Golnaraghi, W.G. Leslie, A. Artegiani, A. Hecht, E. Lazzoni, A. Michelato, E. Sansone, A. Theocharis and Ü. Ünluäta, The eastern Mediterranean general circulation: features, structures and variability, *Dynamics Atmospheres Oceans* 15 (1991) 215–240.
[21] A.R. Robinson and L.J. Walstad, The Harvard open ocean model: Calibration and application to dynamical process, forecasting, and data assimilation studies, *Appl. Numer. Math.* 3 (1–2) (1987) 89–131; also in: R. Vichnevetsky, ed., *Numerical Fluid Dynamics* (North-Holland, Amsterdam, 1987) 89–131.
[22] R. Shapiro, The use of linear filtering as a parameterization for atmospheric diffusion, *J. Atmospheric Sci.* 28 (1971) 523–531.
[23] P.N. Swarztrauber, The methods of cyclic reduction, Fourier analysis and the FACR algorithm for the discrete solution of Poisson's equation on a rectangle, *SIAM Rev.* 19 (1977) 490–501.
[24] P.N. Swarztrauber and R.A. Sweet, Vector and parallel methods for the direct solution of Poisson's equation, *J. Comput. Appl. Math.* 27 (1&2) (1989) 241–263.